Available online at www.sciencedirect.com

SciVerse ScienceDirect

Procedia Engineering 51 (2013) 694 – 702

Procedia Engineering

www.elsevier.com/locate/procedia

Chemical, Civil and Mechanical Engineering Tracks of 3rd Nirma University International Conference (NUiCONE 2012)

Computational study to assess the influence of overlap ratio on static torque characteristics of a vertical axis wind turbine

Sukanta Roy[a], Ujjwal K. Saha[b]*

[a]Research Scholar, Department of Mechanical Engineering, Indian Institute of Technology Guwahati, Guwahati–781039, India
[b]Professor, Department of Mechanical Engineering, Indian Institute of Technology Guwahati, Guwahati–781039, India

Abstract

This paper presents an unsteady two-dimensional computational study in order to observe the effect of overlap ratios on static torque characteristics of a vertical axis wind turbine (VAWT). The study is performed with the help of a finite volume based computational fluid dynamics (CFD) software package Fluent 6.3. The computational model is a two-bladed conventional VAWT having overlap ratios of 0, 0.10, 0.15, 0.20, 0.25 and 0.30. Initially, a comparative analysis is made using various $k-\varepsilon$ turbulence models and then the results are compared with the experimental data available in literature. A realizable $k-\varepsilon$ turbulence model with enhanced wall treatment is found suitable for further computational analysis. The flow field around the turbine model is also studied with the help of static pressure contour analysis. Based on this computational study, it is realized that an overlap ratio of 0.20 eliminates the effects of negative static torque coefficient, provides a low static torque variation at different turbine angular positions and also gives a higher mean static torque coefficient as compared to the other overlap ratios.

Keywords: Vertical axis wind turbine, turbulence model, computational fluid dynamics, overlap ratio, static torque.

Nomenclature

e	Overlap distance between the turbine blades (m)
k	Turbulence kinetic energy (m^2/s^2)
D	Diameter of the turbine (m)
H	Height of the turbine (m)
U	Wind free stream velocity (m/s)
G	Generation of turbulent kinetic energy (m^2/s^2)
Greek symbols	
ε	Energy dissipation rate
δ	Overlap ratio
θ	Rotational angle (degree)
σ	Turbulent Prandtl number
μ	Dynamic viscosity (N-s/m^2)
ρ	Air density (kg/m^3)

* Corresponding author. Tel.: 0091-361-2582663; fax : 0091-361-2690762, 2582699
E-mail address: saha@iitg.ernet.in

doi:10.1016/j.proeng.2013.01.099

1. Introduction

Recent instabilities of world economy, due to the increasing price of carbon-derivative fuels along with the depletion of conventional fuel resources, have stimulated the interest in the generation of renewable energy among the developing countries. One of the most promising concepts is wind energy associated with the local generation of clean electrical energy. Based on the rotational axis, wind turbines are primarily classified as horizontal axis wind turbines (HAWT) and vertical axis wind turbines (VAWT). Nowadays, with the improvement of computational wind engineering, the interest on the VAWTs is greatly enhanced. Nevertheless, these are used as a small scale alternative to wind power extraction because of a variety of reasons such as design simplicity, easy installation, good starting ability, wind direction independency, low operating speed, reduced wear on moving parts and low noise level [1-3].

The Savonius rotor, a kind of drag-type VAWT, consists of two or more semicircular blades with a small overlap between them was conceived by a Finnish engineer, Sigurd Savonius, in 1925, (Fig. 1). This type of wind turbines have a number of applications for local water pumping or small scale power generation, despite their low efficiency compared to lift-driven VAWTs or to modern horizontal axis wind turbines.

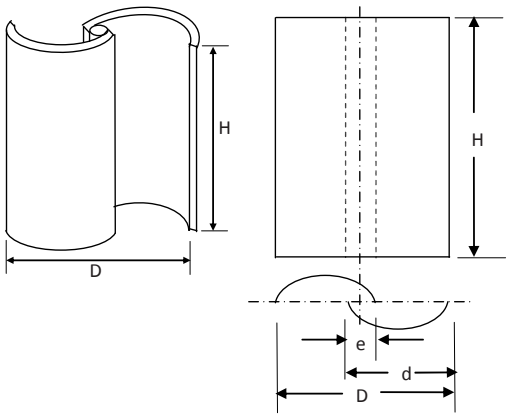

Fig. 1. Schematic diagram of a typical two-bladed VAWT.

The starting ability is of great importance for this type of VAWTs, which is specified by the turbine static torque performance. Savonius turbines can not only work alone but can also serve as the starting auxiliary device for the lift-type Darrieus turbines. However, the static torque of the conventional Savonius turbines has two major drawbacks; one of which is its large static torque variation at various rotor angular positions and the second one is its negative torque value in the 2nd and 4th quarter of the rotor rotational cycle. In order to improve the starting ability of these turbines, several approaches have been taken so far, such as the application of wind shields to reduce the effective static pressure on the returning blade or installing guide vanes to increase the static pressures on the advancing blades [4-6]. However, the wind shields have made the turbine system more complex and wind direction dependent. Saha and Rajkumar [7] have reported a better starting ability of these turbines using twisted blades and observed an optimum blade twisting angle of 15°. A recent study has reported the use of helical blades to increase the starting capability of these turbines and reported positive static torque coefficients at all rotational angles [8]. However, twisted and helical blades also made the system more expensive and complex. Thus, numerous efforts have been made on the guiding mechanisms, twisted blades and helical blades to increase the starting ability of this turbine.

The complex flow phenomena across a drag type VAWT is unsteady in nature. It is often incredible to study this with the help of classical aerodynamic tools such as blade element theory. This gives an account of the use of computational fluid dynamics aimed at determining the flow structure and properties. Although conventionally, experimental methods have formed the backbone of wind turbine research, recent advances in computational techniques have endorsed a new vehicle for turbine study. A reasonably limited amount of simulation work has been shown on drag-type VAWTs. Fujisawa *et al.* [9] have studied the prospects of using CFD through the two-dimensional Reynolds Averaged Navier-Stokes (RANS) CFD simulations on a VAWT, in which steady simulations were conducted to predict the pressure contours and were then compared to the experimentally determined pressures. Altan and Atilgan [10] have conducted steady two-dimensional RANS CFD simulation to forecast the static torque features of a VAWT with a curtain design. Results have shown a good

agreement with the wind tunnel experimental data. In recent times, another two-dimensional computational study has been made on the influence of the blade curve on the turbine performance and reported an optimum turbine design [1].

Several $k-\varepsilon$ turbulence models have been used so far, some are found to be very appreciable to predict flow structure and properties around the VAWTs [11-14]. In this paper, an attempt has been made to study the various $k-\varepsilon$ turbulence models and obtain a suitable model for the analysis of the turbine. Thereafter, with the suitable $k-\varepsilon$ model, investigation has further been made to study the impact of overlap ratio on the static torque performance of a single-stage Savonius type VAWT. A total of six overlap ratios, viz. 0.0, 0.10, 0.15, 0.20, 0.25 and 0.30 have been studied, and the results are compared.

2. Computational methodology

The modeling is carried out with the help of Gambit modeling software for the drag type VAWT as shown in Fig.1. The model has a diameter of 1 m having a height of 1 m and a blade thickness of 0.01 m. The complete two-dimensional computational model includes an inner circle containing the turbine model and an outer rectangle containing the other hollow circle, which exactly fits the inner circle and the turbine model. The computational domain of the rectangle is taken as 2.5 m × 2.5 m. The next step in the simulation effort is the generation of the computational mesh. The unstructured triangular elements were used for meshing the geometry and a good quality mesh was ensured throughout the computational domain using the Gambit mesh generation tool (Fig. 2).

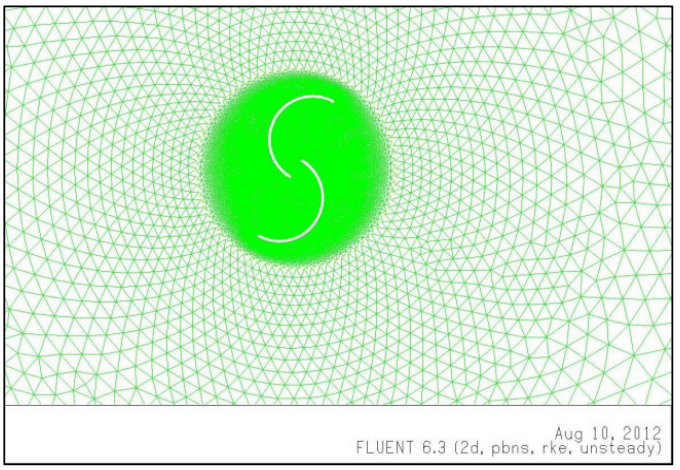

Fig. 2. Grid generation around the vertical axis wind turbine model

While refining the mesh, sufficient care was taken to put additional mesh elements in the regions of high pressure gradient around the blades. Thus, two fluid mesh sections are clearly noticeable; one, adjacent to the turbine blades, very small elements to capture the very sharp velocity gradients at the blade surface and second, the relatively bigger elements in the outer surrounding of the turbine model. In the present analysis, boundary layer was considered and included as the flow is highly turbulent (in the order of 10^5). The y+ value for the boundary layer is achieved to be lesser than 5 for the enhanced wall treatment.

A total of 100000 triangular cells have been taken after the mesh refinement and upon ensuring the non-noticeable difference in the simulation results. The boundary conditions (BC) given to the turbine model are as follows (Fig. 3):

- Inlet: velocity inlet
- Outlet: pressure outlet
- Circles (inner and outer): interface
- Turbine blades: stationary wall

After the Gambit model is prepared and boundary conditions are given, it is exported as a two-dimensional mesh. The mesh file is then imported and analyzed using the CFD-Fluent software.

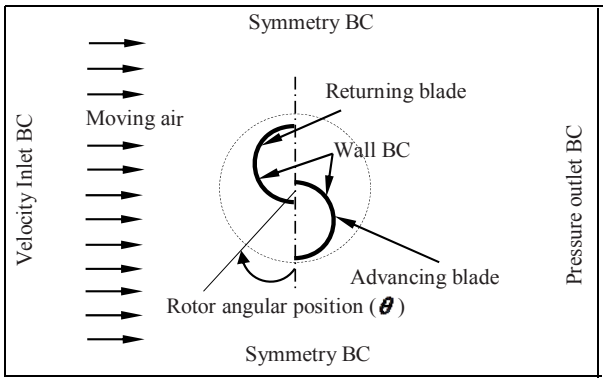

Fig. 3. Boundary conditions given to turbine model in Gambit modeling software

In the flow analysis, the convergence criterion to solve the Navier-Stokes equation is taken as 10^{-3}, whereas 0.001 sec time step size and 20 iterations per time step are taken for the iteration. The mean static torque coefficients are obtained by averaging all the values at different time steps for each angular position, velocity and turbulent model (Fig. 4). The simulation is carried out for 20000 time steps in order to have a number of complete rotations of the turbine model. In this analysis, the following assumptions are made to select the model and the solver:

- Two-dimensional unsteady pressure based solver with 2nd order implicit formulation
- SIMPLE pressure-velocity coupling with 2nd order upwind discretization
- $k-\varepsilon$ turbulence models with enhanced wall functions.

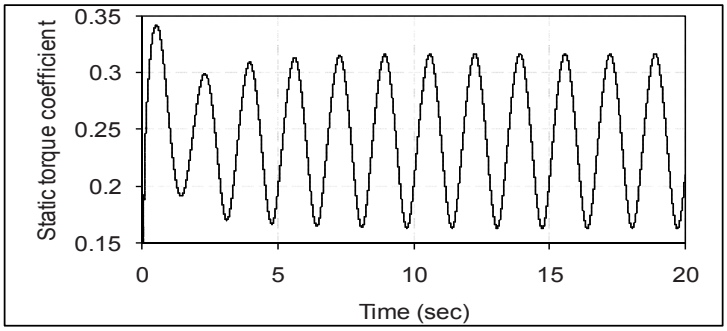

Fig. 4. Static torque coefficients at different time interval of unsteady simulation

Basically, the flow field around a VAWT is highly turbulent. Thus, the main features of turbulence must be considered while choosing the computational technique to solve of a turbulent flow over the turbine model. Therefore, the selection of the turbulence model plays an important role for obtaining the desired computational results. The computational fluid dynamics (CFD) software package Fluent has an option of choosing various $k-\varepsilon$ turbulence models. In order to solve the flow governing equation, the standard $k-\varepsilon$ turbulence model contains the transport formulations for the turbulence kinetic energy (k) and the energy dissipation rate (ε). This two-equation semi-empirical model is expressed as:

$$\frac{\partial}{\partial t}(\rho k)+\frac{\partial}{\partial x_i}(\rho k U_i)=\frac{\partial}{\partial x_j}\left[\left(\mu+\frac{\mu_t}{\sigma_k}\right)\frac{\partial k}{\partial x_j}\right]+G_k+G_b-\rho\varepsilon-Y_M+S_k \quad (1)$$

and

$$\frac{\partial}{\partial t}(\rho \varepsilon)+\frac{\partial}{\partial x_i}(\rho \varepsilon U_i)=\frac{\partial}{\partial x_j}\left[\left(\mu+\frac{\mu_t}{\sigma_\varepsilon}\right)\frac{\partial \varepsilon}{\partial x_j}\right]+C_{1\varepsilon}\frac{\varepsilon}{k}(G_k+C_{3\varepsilon}G_b)-C_{2\varepsilon}\rho\frac{\varepsilon^2}{k}+S_\varepsilon \quad (2)$$

where, G_k denotes the turbulent kinetic energy generation owing to mean velocity gradient, G_b denotes the turbulent kinetic energy generation owing to mean buoyancy, σ_k is the turbulent Prandtl number for k and σ_ε is the turbulent Prandtl number for ε. $C_{1\varepsilon}$, $C_{2\varepsilon}$ $C_{3\varepsilon}$ and C_μ are the constants, whereas, S_k and S_ε are the assumed source terms, Y_M is the effect of the changing dilatation in compressible turbulence to the overall dissipation rate and is expressed as:

$$Y_M = 2\rho\varepsilon\frac{k}{\gamma RT} \tag{3}$$

and the turbulent viscosity (μ_t) is expressed as:

$$\mu_t = \rho C_\mu \frac{k^2}{\varepsilon} \tag{4}$$

The use of standard $k-\varepsilon$ turbulence model has been observed in the investigations of Pope *et al.,* [11] where standard $k-\varepsilon$ model was found to be superior over one equation Spalart-Allmaras turbulence model. The RNG $k-\varepsilon$ model was a consequent of the renormalization group theory and is expressed as:

$$\frac{\partial}{\partial t}(\rho k)+\frac{\partial}{\partial x_i}(\rho k U_i)=\frac{\partial}{\partial x_j}\left[\alpha_k \mu_{eff}\frac{\partial k}{\partial x_j}\right]+G_k+G_b-\rho\varepsilon-Y_M+S_k \tag{5}$$

and

$$\frac{\partial}{\partial t}(\rho \varepsilon)+\frac{\partial}{\partial x_i}(\rho \varepsilon U_i)=\frac{\partial}{\partial x_j}\left[\alpha_k \mu_{eff}\frac{\partial \varepsilon}{\partial x_j}\right]+C_{1\varepsilon}\frac{\varepsilon}{k}(G_k+C_{3\varepsilon}G_b)-C_{2\varepsilon}\rho\frac{\varepsilon^2}{k}-R_\varepsilon+S_\varepsilon \tag{6}$$

By means of a supplementary term R_ε in the ε equation, The RNG model is similar to the standard $k-\varepsilon$ model. Due to this R_ε term in the equation, this model is more reactive to the quick strain properties and streamlines curvature. A better prediction capability of RNG turbulence model has been observed in the available literature [12-14]. Another new development in the $k-\varepsilon$ models is obtained by new formulations of k and ε equations and is recognized as the realizable $k-\varepsilon$ model. The realizable turbulence model is given by:

$$\frac{\partial}{\partial t}(\rho k)+\frac{\partial}{\partial x_j}(\rho k U_j)=\frac{\partial}{\partial x_j}\left[\left(\mu+\frac{\mu_t}{\sigma_k}\right)\frac{\partial k}{\partial x_j}\right]+G_k+G_b-\rho\varepsilon-Y_M+S_k \tag{7}$$

and

$$\frac{\partial}{\partial t}(\rho \varepsilon)+\frac{\partial}{\partial x_j}(\rho \varepsilon U_j)=\frac{\partial}{\partial x_j}\left[\left(\mu+\frac{\mu_t}{\sigma_\varepsilon}\right)\frac{\partial \varepsilon}{\partial x_j}\right]+\rho C_1 S\varepsilon-\rho C_2\frac{\varepsilon^2}{k+\sqrt{\upsilon\varepsilon}}+C_{1\varepsilon}\frac{\varepsilon}{k}C_{3\varepsilon}G_b+S_\varepsilon \tag{8}$$

where, $C_1=\max\left[0.43,\frac{\eta}{\eta+5}\right],\eta=S\frac{k}{\varepsilon},S=\sqrt{2S_{ij}S_{ij}}$

The Realizable $k-\varepsilon$ turbulence model has been widely validated for a variety of flows, which includes rotational shear flows, flow through channels, free flows like jets and mixing layers, boundary layer and separated flows. For number of instances, the prediction capability of this model is found to be significantly improved over that of standard model [15].

3. Results and discussion

In the present study, standard $k-\varepsilon$ turbulence model, renormalized (RNG) $k-\varepsilon$ turbulence model, and realizable $k-\varepsilon$ turbulence model are comparatively studied in order to find their effectiveness to predict the static torque value of VAWTs (Fig. 5). Later, with the suitable turbulence model, computational study is made for a two-bladed VAWT with six overlap ratios from 0.0-0.30.

3.1 Turbulence model selection

The simulations are carried out with these three $k-\varepsilon$ turbulence models for rotor angles in the range of 0°-180° with an angle step of 15°. The computational results using these models are then compared with the experimental data of a two-bladed VAWT with no overlap [16]. Results have shown a better flow prediction with the RNG and realizable $k-\varepsilon$ turbulence models, however, realizable $k-\varepsilon$ model is found to be most suitable (Fig. 5). With the help of realizable $k-\varepsilon$ turbulence model, further computational investigation is made on the effect of overlap ratio for the two-bladed VAWT.

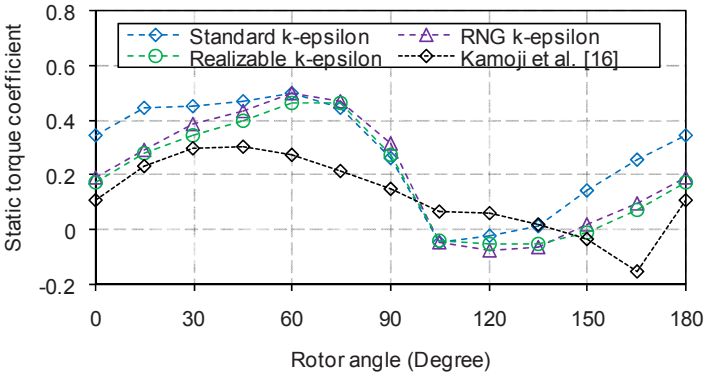

Fig. 5. Comparison of the various $k-\varepsilon$ turbulence models with experimental results at U = 6.96 m/s [16].

3.2 Effect of the overlap ratio

The static torque is a function of the turbine overlap ratio, δ (e/D). In order to study the influence of δ on the turbine starting capability, computational study was made initially for δ = 0.0, 0.10 and 0.15 with the realizable $k-\varepsilon$ turbulence model. Each turbine design is tested for rotor angular positions in the range of 0° to 360° with an angle step of 15°. Results have shown that with the increase of overlap ratio from δ = 0 to 0.15, the turbine static torque performance increases (Figs. 6-9). It is observed that the mean static torque coefficients for a two-bladed rotor with no overlap are 0.189, 0.193, 0.196 and 0.199 at wind free stream velocities, U = 5.57 m/s, 6.69 m/s, 8.35 m/s and 10.44 m/s, respectively.

It is also observed that with no-overlap, the static torque coefficients are found to be negative in the regions of θ = 105°-150° and 285°-330°. Moreover, a large variation in the static torque value at various angular positions is also observed with no overlap. However, with the increase of overlap ratio, this problem diminishes. At wind speeds of 5.57 m/s, 6.69 m/s, 8.35 m/s and 10.44 m/s , the mean static torque coefficients for δ = 0.10 are obtained as 0.202, 0.203, 0.21 and 0.213, respectively; and for δ = 0.15, these values are 0.208, 0.212, 0.217, 0.221, respectively. Thus, a further investigation was intended to observe the influence of higher blade overlap by increasing δ from 0.15 to 0.30 in steps of 0.05.

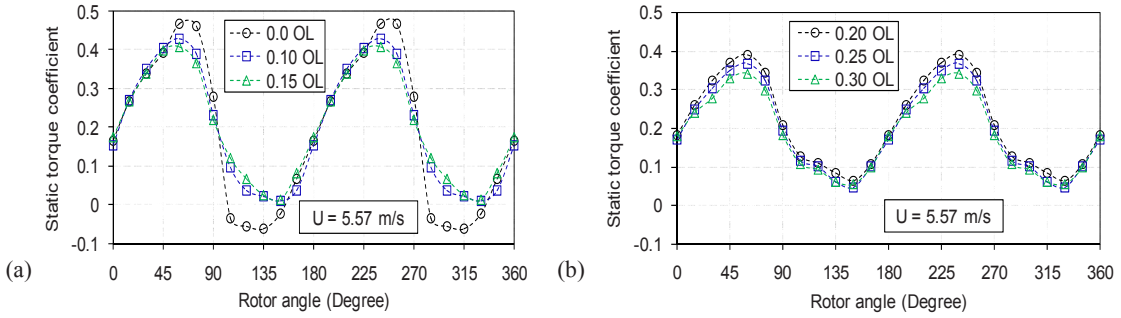

Fig. 6. Effect of the overlap ratios on the turbine static torque characteristics at U = 5.57 m/s for (a) δ = 0.0, 0.10, 0.15 and (b) δ = 0.20, 0.25, 0.30.

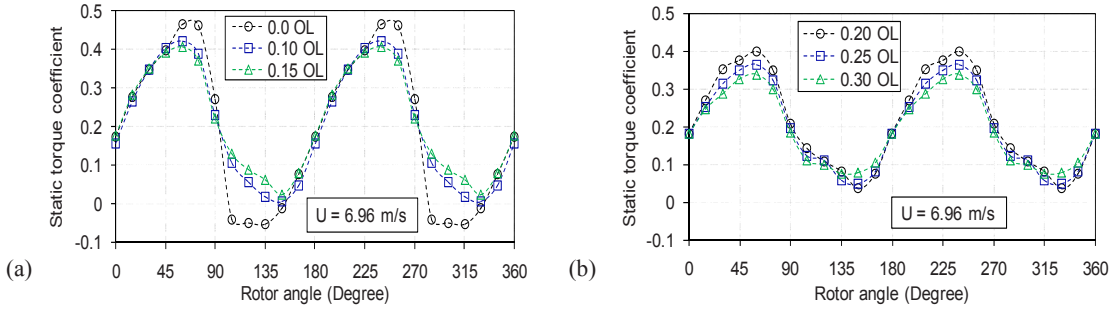

Fig. 7. Effect of the overlap ratios on the turbine static torque characteristics at U = 6.96 m/s for (a) δ = 0.0, 0.10, 0.15 and (b) δ = 0.20, 0.25, 0.30.

With further increase of overlap ratio from 0.15 to 0.30, the mean static torque value increases up to δ = 0.20, and thereafter, it decreases at δ = 0.25 and 0.30. It is observed that at δ = 0.20, the mean static torque coefficient at the tested velocities of U = 5.57 m/s, 6.69 m/s, 8.35 m/s and 10.44 m/s are 0.213, 0.215, 0.218 and 0.224, respectively. For δ = 0.25 and 0.30, these values are 0.197, 0.2, 0.205, 0.21 and 0.188, 0.194, 0.195, 0.199, respectively (Figs. 6-9). The increase in the static torque with the increase of overlap ratio is mainly triggered by the increased pressure on the concave side of the returning blade owing to the flow through the overlap. However, it is realized that as the overlap ratio increases beyond an optimum value, the effective pressure on the concave side of the advancing blade reduces. Thus, at an optimum overlap ratio of 0.20, the peak static torque characteristic of the turbine is observed.

However, it can be noted that the static torque values are increasing with increasing wind speed. At angular positions, at θ=30° to 70° and 210° to 250°; higher values of static torque are observed; whereas, lower values are obtained at angular positions of θ = 105° to 150° and 285° to 330°. These variations of high and low static torques are also observed in the available literature [1, 2, 17].

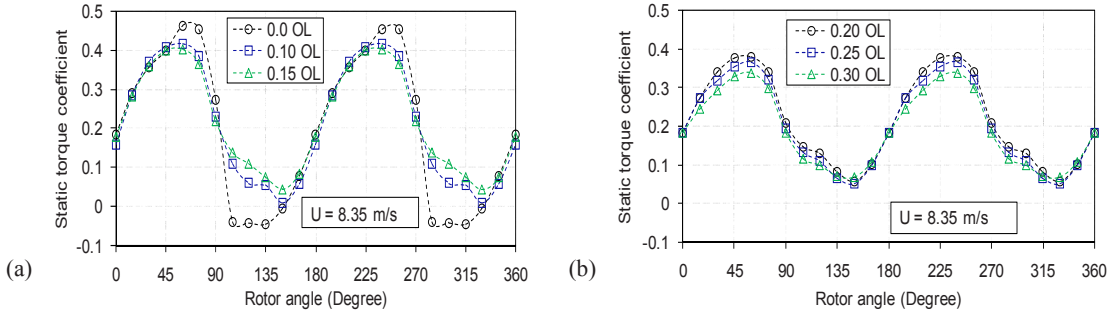

Fig. 8. Effect of the overlap ratios on the turbine static torque characteristics at U = 8.35 m/s for (a) δ = 0.0, 0.10, 0.15 and (b) δ = 0.20, 0.25, 0.30.

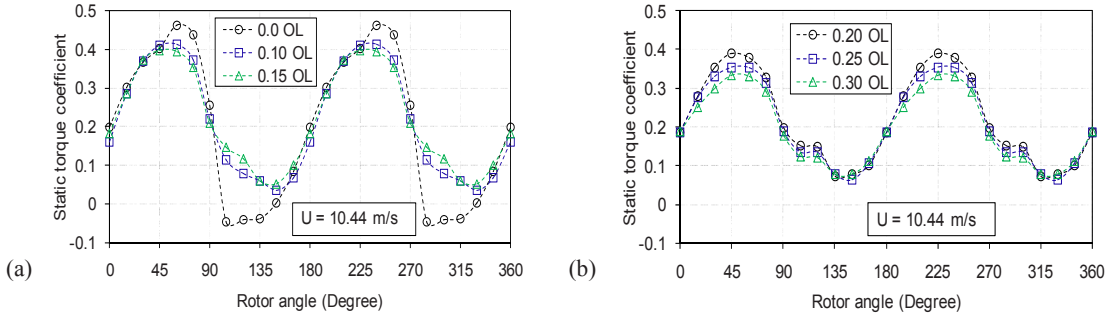

Fig. 9. Effect of the overlap ratios on the turbine static torque characteristics at U = 10.44 m/s for (a) δ = 0.0, 0.10, 0.15 and (b) δ = 0.20, 0.25, 0.30.

Fig. 10 shows the variations of average static torque coefficients with the variation of overlap ratios in the range of 0.0 to 0.30. It is shown for different wind free-stream velocities from 5.57 to 10.44 m/s. The results have shown that with the increase of wind free stream velocity, the mean static torque coefficients are also increasing. It has been observed that the average static torque coefficient increases with the increase of overlap ratio up to 0.20 and beyond this, again it decreases. The major drawback of large variation in torque coefficient is also reduced with the increase of overlap. Besides, a positive static torque value is achieved for all angular positions with the higher overlap ratios.

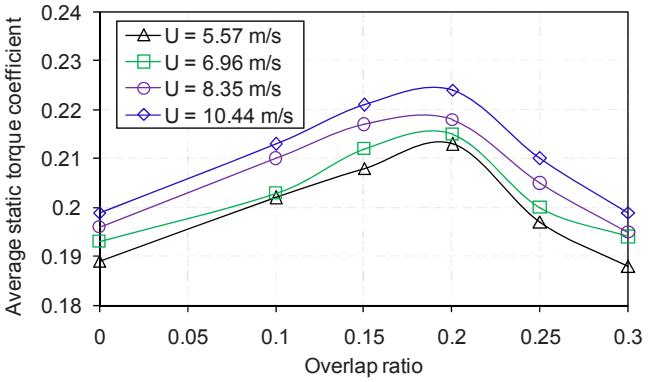

Fig. 10. Effect of overlap ratios on the average static torque coefficient for a two-bladed VAWT.

Fig. 11 shows the static pressure distribution around the turbine blades at different angular positions (θ) with an overlap ratio of 0.20. This static pressure is responsible for the turbine static torque generation. At θ= 0°, a comparatively lower value of static pressure in the returning blade and a higher value on the advancing blade of the turbine are observed. Thus, it gives a moderate value of positive static torque. As the value of θ increases, the value of static pressure on the advancing blade also increases, and consequently, the static pressure on the returning blade decreases. At θ= 30° to 70°, the net static pressure, and hence, the net static torque experiences a higher value. On the other side, at angular positions in the range of, 105°< θ<150°, a high static pressure on the returning blade and a low value on the advancing blade of this VAWT are experienced. Thus, the static torque coefficients are observed lower in this region. These findings also confirm the results shown in Figs. 6 through 9.

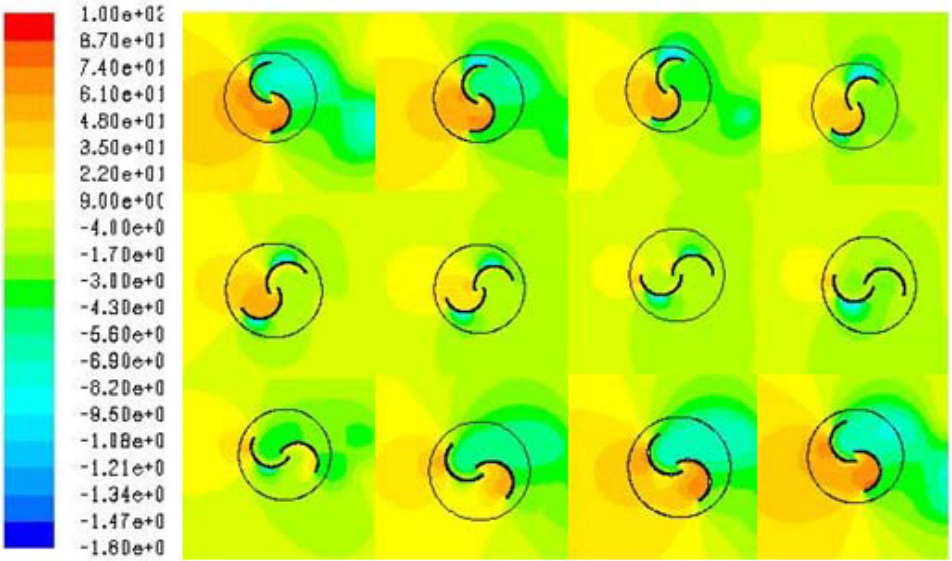

Fig. 11. Static pressure contours at various angular positions at δ = 0.20.

4. Conclusion

In this paper, two-dimensional unsteady simulations were carried out to investigate the effect of overlap ratios on the static torque performance of a drag based VAWT of Savonius type. A realizable $k-\varepsilon$ turbulence model is observed to be the superior among the various $k-\varepsilon$ turbulence models tested. While considering the turbine starting ability, the large variation of the static torques at various angular positions from $\theta = 0°$ to 360° and the negative torque values at the 2nd and 4th quarter of the turbine rotational cycle were the major drawback for this turbine. However, from this computational study, it is observed that with the increase in the blade overlap, positive static torque coefficients are recognized in the complete rotational cycle of this turbine. As the overlap ratio increases at a value of 0.20, the large variation of the static torques at various angular positions is also reduced. An optimum mean static torque coefficient of 0.224 is obtained with $\delta = 0.20$ at $U = 10.44$ m/s. The increase of the static torque with the increase of overlap ratio is mainly due to increased pressure on the concave side of the turbine returning blade. Moreover, it is seen that with an increase of overlap ratio beyond 0.20, the mean static torque coefficient value decreases, although a positive value of static torque coefficient is observed over the complete 360° rotation. These reductions beyond $\delta = 0.20$ are mainly due to reduced pressure on the concave side of the rotor advancing blade. At angular positions of $\theta = 30°$ to 70° and 210° to 250°, higher values of static torque coefficients are observed, whereas, lower static torque coefficients are obtained at $\theta = 105°$ to 150° and 285° to 330°.

References

[1] Kianifar, A., Anbarsooz, M., 2011. "Blade curve influences on the performance of Savonius rotors: experimental and numerical," Proceedings of the Institution of Mechanical Engineers, Part A: Journal of Power and Energy 225, pp. 343-350.

[2] Sargolzaei, J., Kianifar, A., 2009. Modeling and Simulation of Wind Turbine Savonius Rotors Using Artificial Neural Networks for Estimation of the Power Ratio and Torque, Simulation Modelling Practice and Theory 17, pp. 1290-1298.

[3] Li, Y., Feng, F., Li, S., Han, Y., 2010. "Computer simulation on the performance of a combined-type Vertical axis wind turbine," Proceedings of the International Conference on Computer Design and Applications 4, IEEE Xplore, pp. 247-250.

[4] Altan, B.D., Atilgan, M., Ozdamar, A., 2008. An Experimental Study on Improvement of a Savonius Rotor Performance with Curtaining, Experimental Thermal and Fluid Sciences 32, pp. 1673-1678.

[5] Shikha, Bhatti, T.S., Kothari, D.P., 2003. Vertical Axis Wind Rotor with Concentration by Convergent Nozzles, Wind Engineering 27, pp. 555-559.

[6] Mohamed, M.H., Janiga, G., Pap, E., Thevenin, D., 2010. Optimization of Savonius Turbines Using an Obstacle Shielding the Returning Blade, Renewable Energy 35, pp. 2618-2626.

[7] Saha, U.K., Rajkumar, M.J., 2006. On the Performance Analysis of Savonius Rotor with Twisted Blades, Renewable Energy 31, pp. 1776-1788.

[8] Kamoji, M.A., Kedare, S.B., Prabhu, S.V., 2009. Performance Tests on Helical Savonius Rotor, Renewable Energy 34, pp. 521-529.

[9] Fujisawa, N., Ishimatsu, K., Kage, K., 1995. A Comparative Study of Navier-Stokes Calculations and Experiments for the Savonius Rotor, Journal of Solar Energy 117, pp. 344-346.

[10] Altan, B.D., Atilgan, M., 2008. An Experimental and Numerical Study on the Improvement of the Performance of Savonius Wind Rotor, Energy Conversion and Management 49, pp. 3425-3432.

[11] Pope, K., Rodrigues, V., Doyle, R., Tsopelas, A., Gravelsins, R., Naterer, G.F., Tsang, E., 2010. Effects of Stator Vanes on Power Coefficients of a Zephyr Vertical Axis Wind Turbine, Renewable Energy 35, pp. 1043-1051.

[12] Emmanuel, B., Jun, W., 2011. Numerical Study of a Six-Bladed Savonius Wind Turbine, Journal of Solar Engineering 133, pp. 1-5.

[13] McTavish, S., Feszty, D., Sankar, T., 2012. Steady and Rotating Computational Fluid Dynamics Simulations of a Novel Vertical Axis Wind Turbine for Small-Scale Power Generation, Renewable Energy 41, pp. 171-179.

[14] Yonghai, H.U., Zhengmin, T., Shanshan, W., 2009. "A new type of VAWT and blade optimization," Proceedings of the International Conference on Technology and Innovation, IEEE Xplore, pp. 1-5.

[15] Kim, S.E., Choudhury, D., Patel, B., 1997. "Computations of complex turbulent flows using the commercial code FLUENT," Proceedings of the ICASE/LaRC/AFOSR Symposium on Modeling complex turbulent flows, Kluwer Academic Publishers, pp. 259-276.

[16] Kamoji, M.A., Kedare, S.B., Prabhu, S.V., 2009. Experiments Investigations on Single Stage Modified Savonius Rotor, Applied Energy 86, pp. 1064-1073.

[17] Fujisawa, N., Gotoh, F., 1992. Pressure Measurements and Flow Visualization Study of a Savonius Rotor, Journal of Wind Engineering and Industrial Aerodynamics 39, pp. 51-60.